PAPER

Effects of electron trapping on nonlinear electron-acoustic waves excited by an electron beam via particle-in-cell simulations

Plasma Sci. Technol. **21** (2019) 055301 (9pp) https://doi.org/10.1088/2058-6272/ab033f

Effects of electron trapping on nonlinear electron-acoustic waves excited by an electron beam via particle-in-cell simulations

A A ABID[1,4], **Quanming LU** (陆全明)[1,4], **Huayue CHEN** (陈华岳)[1], **Yangguang KE** (柯阳光)[1], **S ALI**[2,3] **and Shui WANG** (王水)[1]

[1] CAS Key Laboratory of Geospace Environment, Department of Geophysics and Planetary Science, University of Science and Technology of China, Hefei 230026, People's Republic of China
[2] National Centre for Physics (NCP) at Quaid-e-Azam University Campus, Shahdra Valley Road, Islamabad 44000, Pakistan
[3] Hefei National Laboratory for Physical Sciences at the Microscale and Department of Physics, University of Science and Technology of China, Hefei 230026, People's Republic of China

E-mail: abidaliabid1@hotmail.com and qmlu@ustc.edu.cn

Received 18 October 2018, revised 28 January 2019
Accepted for publication 29 January 2019
Published 26 March 2019

Abstract

By performing one-dimensional particle-in-cell simulations, the nonlinear effects of electron-acoustic (EA) waves are investigated in a multispecies plasma, whose constituents are hot electrons, cold electrons, and beam electrons with immobile neutralized positive ions. Numerical analyses have identified that EA waves with a sufficiently large amplitude tend to trap cold electrons. Because EA waves are dispersive, where the wave modes with different wavenumbers have different phase velocities, the trapping may lead to the mixing of cold electrons. The cold electrons finally get thermalized or heated. The investigation also shows that the excited EA waves give rise to a broad range of wave frequencies, which may be helpful for understanding the broadband-electrostatic-noise spectrum in the Earth's auroral region.

Keywords: electron acoustic waves, cold electrons trapping, particle-in-cell (PIC) simulation

(Some figures may appear in colour only in the online journal)

1. Introduction

Electron-acoustic (EA) waves are the longitudinal waves that exist in a plasma composed of hot and cold electron components [1–4] and have been widely used to explain the broadband-electrostatic-noise (BEN) observed in the Earth's and other planetary magnetosphere [5–8]. In particular, Fried and Gould [9] presented numerical solutions of the electrostatic dispersion relation in an unmagnetized uniform plasma and predicted the existence of EA waves exhibiting distinct acoustic-like properties. Later, Watanabe and Taniuti [10] studied several novel features of EA waves with two distinct components of electrons (viz., cold electrons and hot electrons) having different numbers of densities and temperatures. EA waves are strongly Landau damped because the electron thermal speed is almost equivalent to the phase velocity [11] of the wave and its damping decreases when the hot and cold electron temperature ratio is very large. The frequency of EA waves is essentially larger than that of ion acoustic waves and less than Langmuir waves, while its phase velocity intermediates the cold and hot electron thermal speeds [12, 13]. Gary and Tokar [14] presented the dispersive properties of linear EA waves in a uniform unmagnetized Vlasov plasma and demonstrated a necessary criterion: the temperature ratio of hot to cold electron is larger than a factor of 10.

EA waves can be excited by a tenuous electron beam moving along the magnetic field direction in a plasma with hot and cold electron components [15, 16]. Moreover, the investigation of nonlinear electrostatic waves with an electron beam was first observed by the Fast Auroral Snapshot (FAST) spacecraft [17] and later by the Polar spacecraft [18]. Since hot, cold, and beam electrons strongly contribute to the electrostatic waves, they have received a great deal of attention in elucidating

[4] Author to whom any correspondence should be addressed.

the BEN in the Earth's auroral region. It has been found that nonlinear features play a significant role in the generation of BEN and the frequency of the BEN emission is vividly larger than the electron plasma frequency. The high-frequency part of the BEN is normally described by the frequency spectrum generated by the electrostatic solitons [19, 20]. Specifically, El-Taibany and Moslem [21] explained the higher order nonlinearity and dispersion effects involving EA waves and examined collective interactions of electron beam and higher order nonlinearity on the profiles of EA solitary waves by utilizing the well-known reductive perturbation technique.

Tokar and Gary [15] carried out numerical simulations for the stability of electrostatic and electromagnetic waves in the dayside polar cusp and analyzed an electrostatic instability due to beam electrons. Later, Matsukiyo *et al* [22] employed a one-dimensional (1D) particle-in-cell (PIC) simulation formalism to examine high-frequency waves in an auroral upward current region and illustrated ion acoustic (IA) and electron two-stream Langmuir in the nonlinear state. Berthomier *et al* [23] utilized a non-perturbative technique to study nonlinear EA waves with electron beam in an unmagnetized plasma. Lu *et al* [24] proposed a plasma system to investigate the nonlinear behavior of the electrostatic waves using a numerical approach commonly identified as a '1D electrostatic PIC simulation'.

Electrons may be trapped by large amplitude electrostatic waves and result in nonlinear effects such as steepening and electron phase-space holes. The typical steepening can occur in the gases [25], magnetosonic [26], ion acoustic [27], and dust acoustic [28] waves. Electron phase-space holes are formed due to trapping of electrons in a potential well of phase-space holes and the associated electrostatic structures usually have a symmetric bipolar parallel (aligned magnetic field) electric field [17, 29].

Recently, Abdelwahaed *et al* [30] employed the reductive perturbation technique to study auroral EA waves with trapped vortex hot electrons and derived a perturbed higher order modified Korteweg−de Vries equation with electron temperature and trapping effects on the electro-field and energy in auroral plasmas. Cylindrical EA solitons were later investigated in vortex plasmas [31], while the propagation of small amplitude EA solitary and shock waves [32] in unmagnetized dissipative plasma accounting for cold electron fluid, nonextensive super thermal hot electrons and static ions.

However, at ion dynamical scale, Hafez *et al* [33] studied nonlinear obliquely propagating IA waves in an unmagnetized fully ionized plasma with trapped electrons, hot ions, and Boltzmann positrons. They not only derived a modified Kadomtsev−Petviashivili equation but also an energy integral equation, showing a parametric variation of phase speed, Sagdeev potential, amplitude, and width of solitary pulses.

In this paper, with a 1D PIC simulation model, we examine the nonlinear effects when sufficiently large amplitude EA waves are excited by an electron beam in a plasma of cold and hot electrons. The electrons are then trapped by the EA waves which at last cause an obvious mixing and heating of the cold electrons. This paper is organized as follows: In section 2, we present a theoretical and simulation formalism for an unmagnetized three-component plasma and discuss the generalized dispersion relation of electrostatic waves with specific limiting cases for numerical analysis. Section 2 explains the basic parameters of the 1D PIC simulation model and section 3 analyzes the simulation results. We end this article with a summary in section 4.

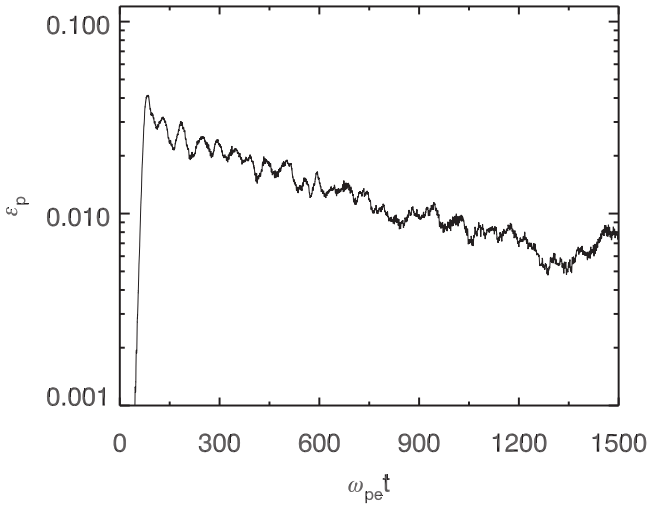

Figure 1. Normalized electric (E_x) field energy ($\varepsilon_p = E^2\varepsilon_0/2k_BT_cn_0$) in log scale versus time evolution ($\omega_{pe}t$) for run 1.

Table 1. Simulation parameters for runs 1–4 with $n_{h0}/n_{c0} = 1$.

Run	T_h/T_c	T_h/T_b	n_{b0}/n_0	n_{c0}/n_0	u_d/V_{Tc}
1	100	100	0.02	0.49	20
2	100	100	0.02	0.49	8.0
3	10.0	10.0	0.02	0.49	20
4	100	100	0.04	0.48	20

2. Theoretical and simulation formalisms

We consider a collisionless unmagnetized uniform plasma, whose constituents are hot, cold, and beam electrons as well as positive ions. The massive ions are assumed as immobile which only appear through the charge-neutrality condition $n_{i0} = n_{e0} = n_0$ with $n_0 = n_{h0} + n_{c0} + n_{b0}$ where n_{j0} represents the equilibrium charge density of the jth plasma species (j = h for hot electrons, c stands for cold electrons, and b stands for beam electrons). All the electrons initially follow the standard Maxwellian distribution. However, beam electrons in particular move with a drift speed (u_d) along the x-axis. The dynamics of the electrostatic waves can be expressed by the following linearized set of Vlasov−Poisson equations [34]:

$$\left(\frac{\partial}{\partial t} + \mathbf{v}_j.\nabla\right)f_{j1} - \frac{q_j}{m_j}\nabla\phi_1.\nabla_{\mathbf{v}}f_{j0} = 0 \qquad (1)$$

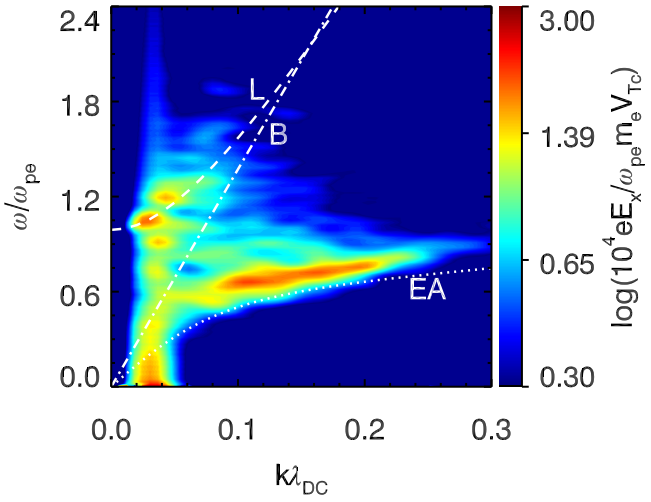

Figure 2. The ω-k diagram at $\omega_{pe}t = 1\ 200$–$1\ 400$ for run 1. The EA, L, and B curves represent dispersion relations for the electron acoustic, Langmuir, and beam driven waves, respectively.

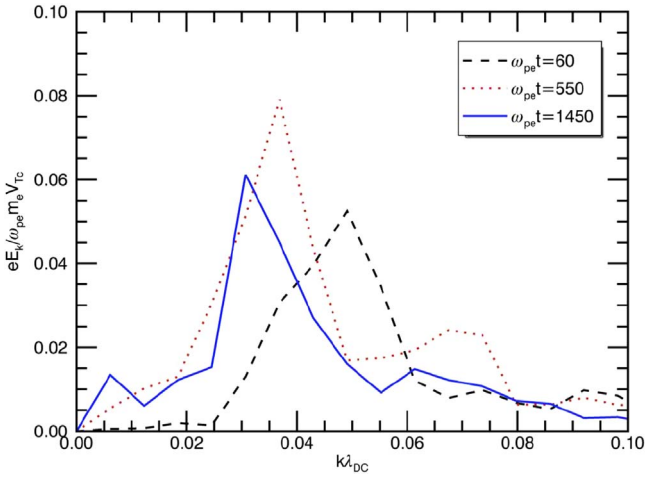

Figure 3. Normalized electric field E_k vs. k at $\omega_{pe}t = 60$, 550, and 1450 for run 1.

and

$$-\nabla^2\phi_1 = 4\pi\sum_j q_j \int f_{j1}\,\mathrm{d}\mathbf{v}_j, \tag{2}$$

where $f_{j1}(\ll f_{j0})$ denotes the perturbed (equilibrium) distribution function and ϕ_1 is the induced electrostatic potential. Applying Fourier transformations to equations (1) and (2), we finally reach $D(\omega, k)\phi_1 = 0$, where the dielectric response function for the electrostatic waves is given by [35]

$$D(\omega, k) = 1 + \sum_{j=\mathrm{h,c,b}} \frac{2}{k^2\lambda_{\mathrm{D}j}^2}[\xi_j Z(\xi_j) + 1] \tag{3}$$

where $\xi_j = (\omega - ku_{\mathrm{d}j})/kV_{Tj}$ is a dimensionless variable, which contains zero hot- and cold-electron drift speeds $u_{\mathrm{dh}} = u_{\mathrm{dc}} = 0$ with a non-zero beam electron drift speed $u_{\mathrm{db}} \neq 0$. The plasma oscillation frequency, Debye length, and thermal velocity of the jth species are, respectively, defined

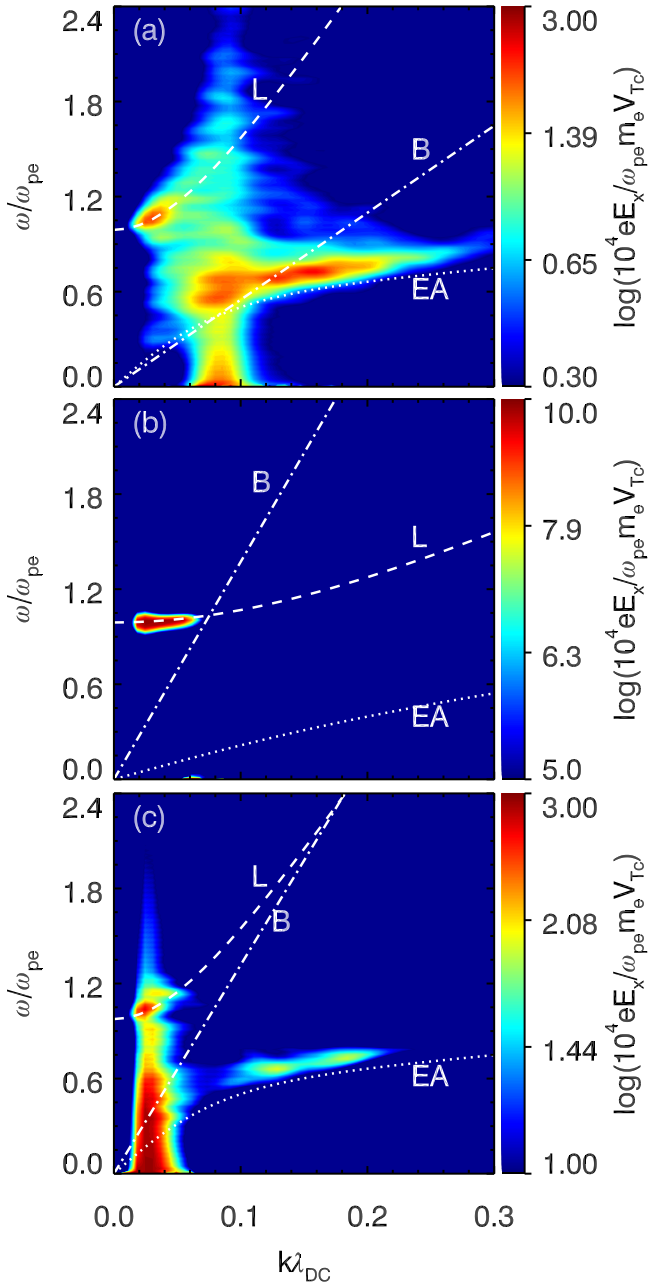

Figure 4. The ω-k diagram at $\omega_{pe}t = 1200 - 1400$ for (a) run 2, (b) run 3, and (c) run 4.

by $\omega_{pj}[=(n_{j0}q_j{}^2/m_j\varepsilon_0)^{1/2}]$, $\lambda_{\mathrm{D}j}[=(\varepsilon_0 k_{\mathrm{B}} T_j/q_j{}^2 n_{j0})^{1/2}]$, and V_{Tj} $[=(2T_j/m_j)^{\frac{1}{2}}]$. T_j stands for temperature (in energy unit) and $Z(\xi_j)$ refers to the plasma dispersion function for plasma species [33]. Assuming that the beam electron density is much smaller than the total electron density, viz., $n_{\mathrm{b0}} \ll n_{\mathrm{e0}}$ with $\xi_{\mathrm{h}} \ll 1$ and $\xi_{\mathrm{c}} \gg 1$, equation (3) accordingly gives the dispersion relation of EA waves at the cold-electron timescale [14], as

$$\omega^2 = \omega_{\mathrm{pc}}^2 \frac{k^2\lambda_{\mathrm{Dh}}^2(3k^2\lambda_{\mathrm{Dc}}^2 + 1)}{k^2\lambda_{\mathrm{Dh}}^2 + 1}. \tag{4}$$

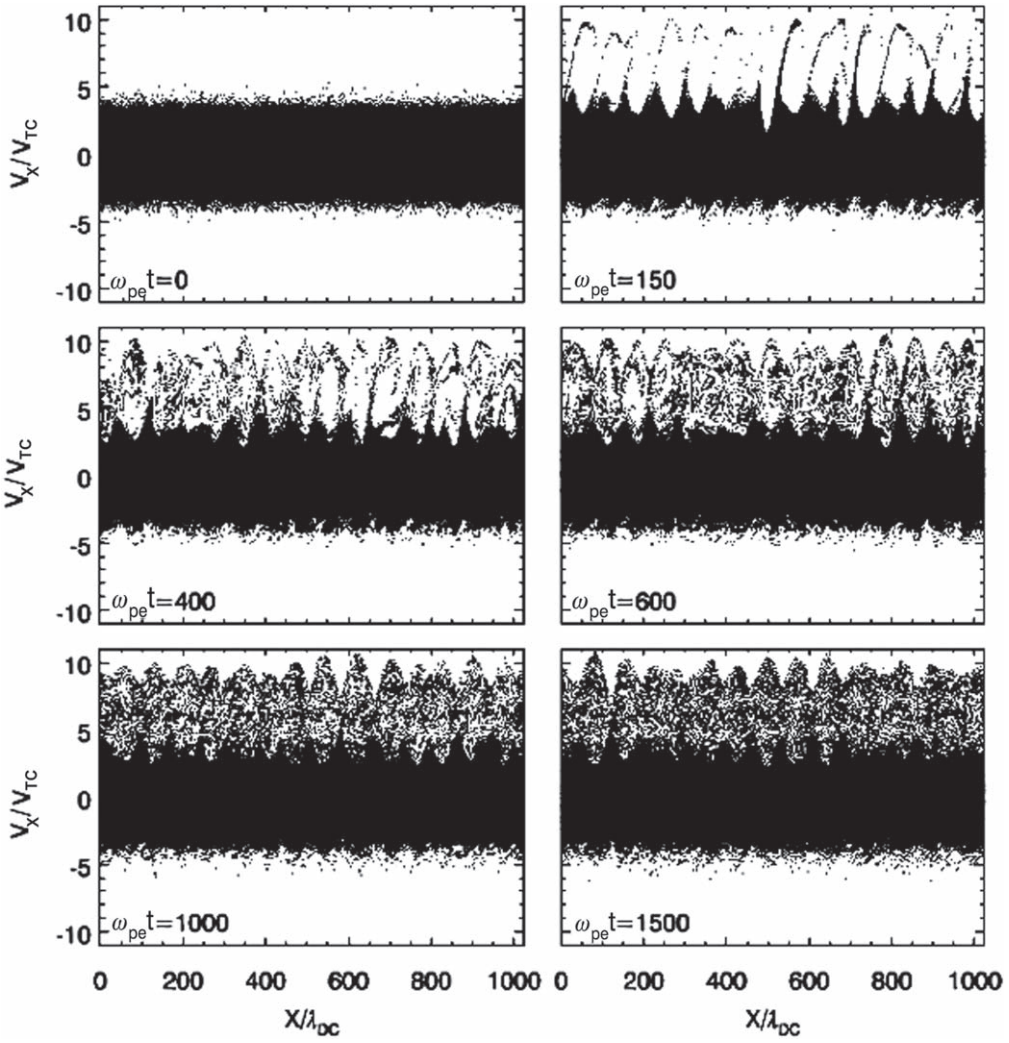

Figure 5. The phase-space (x, v_x) plots for the cold electrons at $\omega_{pe}t$ = 0, 150, 400, 600, 1 000, and 1 500 for run 2.

On the other hand, we use $\xi_h \gg 1$ in equation (3) to obtain the dispersion relation of the electron plasma waves (Langmuir waves) as [36]

$$\omega^2 = \omega_{ph}^2(3k^2\lambda_{Dh}^2 + 1) + \omega_{pc}^2(3k^2\lambda_{Dc}^2 + 1), \quad (5)$$

where ω_{ph} and ω_{pc} are the hot and cold plasma oscillation frequencies, respectively. For the finite beam electron streaming speed $u_{db} = u_d \neq 0$, the dispersion relation (3) may be reduced to

$$1 - \frac{\omega_{ph}^2}{\omega^2} - \frac{\omega_{pc}^2}{\omega^2} - \frac{\omega_{pb}^2}{(\omega - ku_d)^2} = 0, \quad (6)$$

where ω_{pb} is the plasma frequency due to beam electrons. In the limit, when the electrons beam density (n_{b0}) is much smaller than the total electron density (n_0), equation (6) then becomes

$$\omega = \frac{Ku_d}{1 + n_b/n_0} \approx ku_d. \quad (7)$$

This represents a mode of the beam driven wave.

To investigate the nonlinear properties of EA waves, we consider an electrostatic 1D PIC simulation model, which only permits spatial variations along the x-axis [37]. The ambient magnetic field is neglected in this model. Initially, the plasma particles are loaded into the grids with a Maxwellian velocity distribution. The positions and velocities of the plasma particles progress from the previous point by a little time step utilizing the latest fields. The applied boundary conditions are periodic. The unperturbed densities of hot electrons (n_{h0}), cold electrons (n_{c0}), and beam electrons (n_{b0}) are normalized by the whole unperturbed electron density $n_{e0}[=n_{h0} + n_{c0} + n_{b0}]$, while the electron velocities are articulated in the unit V_{Tc} (cold electron thermal velocity). The space (x) and time (t) are normalized by the Debye length of cold electrons $\lambda_{Dc}[=(\varepsilon_0 k_B T_c/e^2 n_{c0})^{1/2}]$ and the inverse of the plasma frequency ω_{pe} $[=(n_{e0}e^2/m\varepsilon_0)^{1/2}]$, respectively. The axial electric field (E_x) and potential ϕ have been normalized by $\omega_{pe}V_{Tc}m_e/e$ and $k_B T_c/\varepsilon_0 e$, respectively. In this

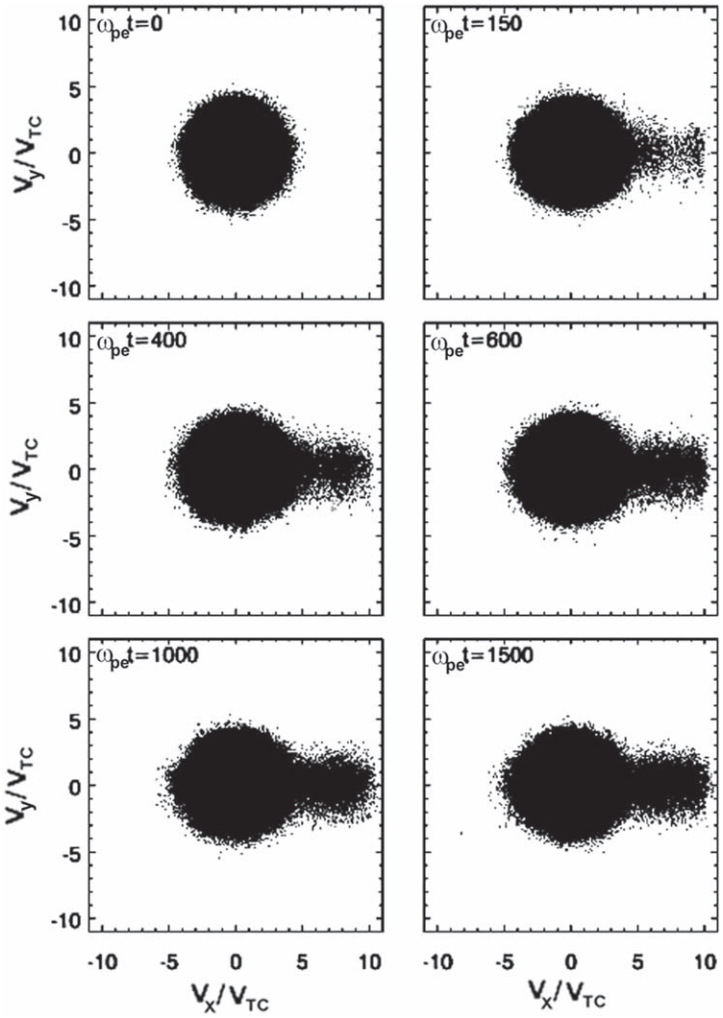

Figure 6. The space (v_x, v_y) plots for the cold electrons at $\omega_{pe}t$ = 0, 150, 400, 600, 1 000, and 1 500 for run 2.

simulation, we have utilized the total number of particles 13 107 200 and total number of grid cells 1 024 with a grid size equal
to the cold-electron Debye length λ_{Dc}. A fixed time step $dt = 0.02\ \omega_{pe}^{-1}$ and spatial step $dx = 1\ \lambda_{Dc}$ are also chosen in our simulations.

3. Simulation results

In this paper, we perform 1D PIC simulations with variation of plasma parameters to study the nonlinear effects of EA waves. The parameters are given in the table 1, which shows that PIC simulations are carried out for four runs. Run 1 is taken as a benchmark case because the existence of waves has been inferred from it. Figure 1 represents the plot of the normalized electric field energy ($\varepsilon_p = E^2\varepsilon_0/2k_BT_cn_0$) on the logarithmic scale as a function of the normalized time ($\omega_{pe}t$). Note that the electric field energy increases exponentially and reaches $\varepsilon_p \sim 0.0414$ at $\omega_{pe}t = 84.12$. When $\omega_{pe}t$ goes beyond the value 84.12, the magnitude of the electric field energy changes little, showing the nonlinear stage.

By applying the Fourier transform to E_x both in time and space within the temporal range $\omega_{pe}t$ = 1 200–1 400, we display the ω-k dispersion diagram in figure 2, where the electrostatic waves, for example, EA waves, beam driven (B) waves, and Langmuir (L) waves are excited in the simulation results. The linear dispersion curves are derived from equations (4)–(6) for identifying the simulation results. Here the dashed curve represents a Langmuir wave, the dashed −dotted curve corresponds to the beam driven wave, and the dotted curve shows the EW wave. For an intermediate range of $k\ \lambda_{Dc}$ = 0.08–0.25, the EA wave becomes more prominent at the cold electron timescale following an acoustic behavior. However, the frequency of the L waves is larger than the B waves but the B waves have a broad spectrum of frequency because the beam speed almost resonates with the phase speed of the B waves. It can be noted that the EA wave mode shows a large amplitude with a broad wavenumber, damps strongly for a large wavenumber and weakly at small wavenumber. Theoretically, the curves of the Langmuir and beam driven waves intersect each other in a regime where both are strongly damped. Figure 3 represents how the Fourier transformed electric field (E_k) varies with a normalized wavenumber (k) for different values of $\omega_{pe}t$(=60, 550, and 1 450)

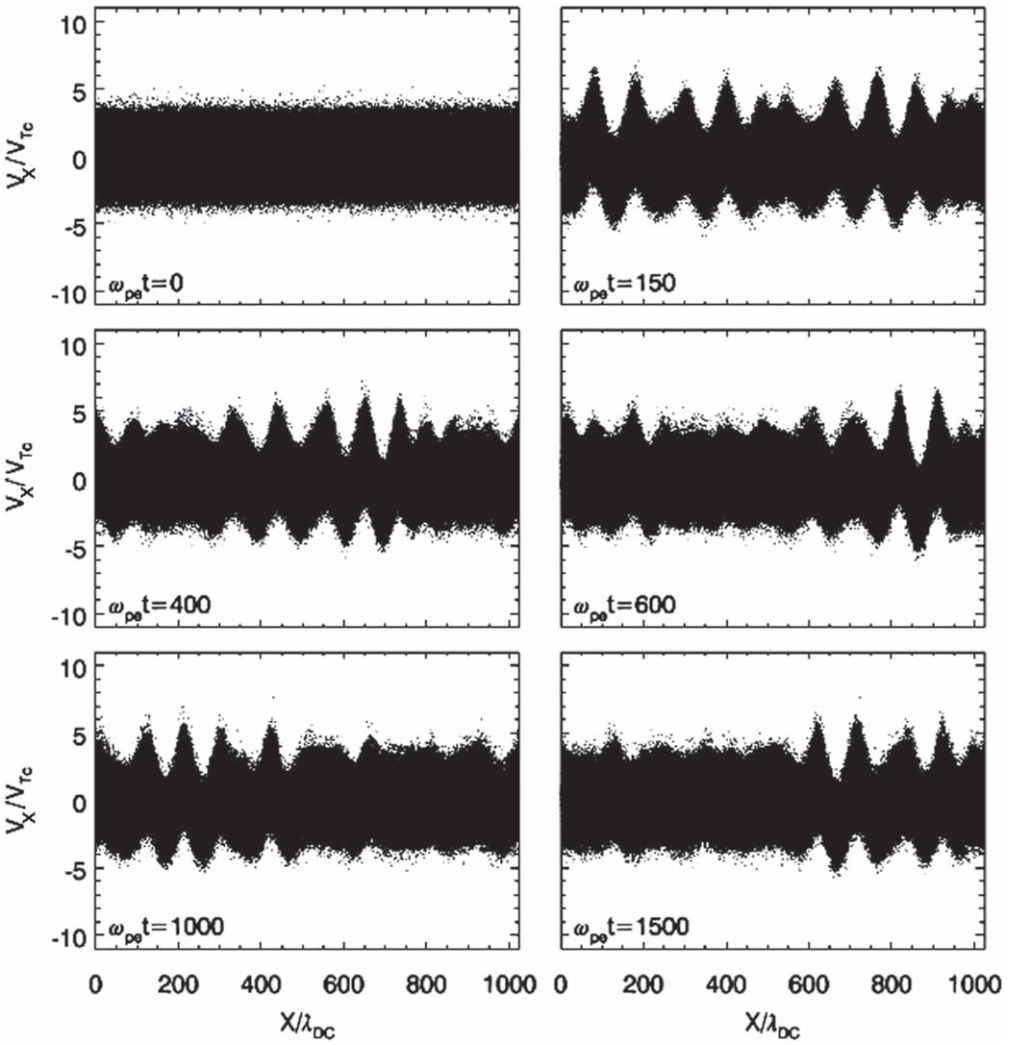

Figure 7. The phase-space (x, v_x) plots for the cold electrons at $\omega_{pe}t$ = 0, 150, 400, 600, 1 000, and 1 500 for run 3.

in run 1. It has been observed that the peaks of the curves shift toward the origin when the value of the normalized time ($\omega_{pe}t$) increases.

The dispersion diagrams constructed for the variation in certain plasma parameter, such as the electron beam streaming speed, hot electron temperature, and beam electron density are displayed in figures 4(a)–(c). Figure 4(a) examines the effect of the electron drift speed (u_d) at $8V_{Tc}$ for run 2. Other parameters utilized here are the same as those in the run 1. It is observed that the reduction in the value of u_d leads to the mitigation the amplitude of the B wave and consequently the EA wave becomes dominant. We now decrease the hot electron temperature and increase the beam density in figures 4(b) and (c), respectively. See that the ω-k dispersion diagram for run 3, where all the parameters are taken, are the same as that of run 1, except for the hot electron temperature [$T_h/T_c = 10$], which is now clearly displayed in figure 4(b). It has been noted that by decreasing the hot electron temperature only the L waves are observed to be in the prominent mode due to its small Landau damping rate. In run 4, we have changed the beam electron density ($n_{b0}/n_0 = 0.04$) while keeping $n_{h0}/n_{c0} = 1$ and the other parametric values of run 1 as they are. It has been found that by increasing the beam electron density, the amplitude of the B waves increases while the EA and L waves damp.

To examine the influence of cold electrons on the EA waves, figure 5 exhibits the normalized phase-space (x, v_x) coordinates for different normalized times $\omega_{pe}t$ (=0, 150, 400, 600, 1 000, and 1 500) by using the plasma parameters of run 2 from table 1. We have noticed that initially at $\omega_{pe}t = 0$, the cold electrons follow a Maxwellian velocity distribution. For finite times, the wave−particle interaction leads to nonlinear structures in the form of vortices. The waves attain a saturation level from the normalized times 1 000−1 500. Consequently, part of the cold electrons became trapped in the waves, and these trapping vortices become prominent. Since the electron-acoustic wave appears to be the more dominant mode (see figure 4(a)) in run 2, therefore the large amplitude of the electron-acoustic waves tends to trap the cold electrons more effectively. As the EA waves are

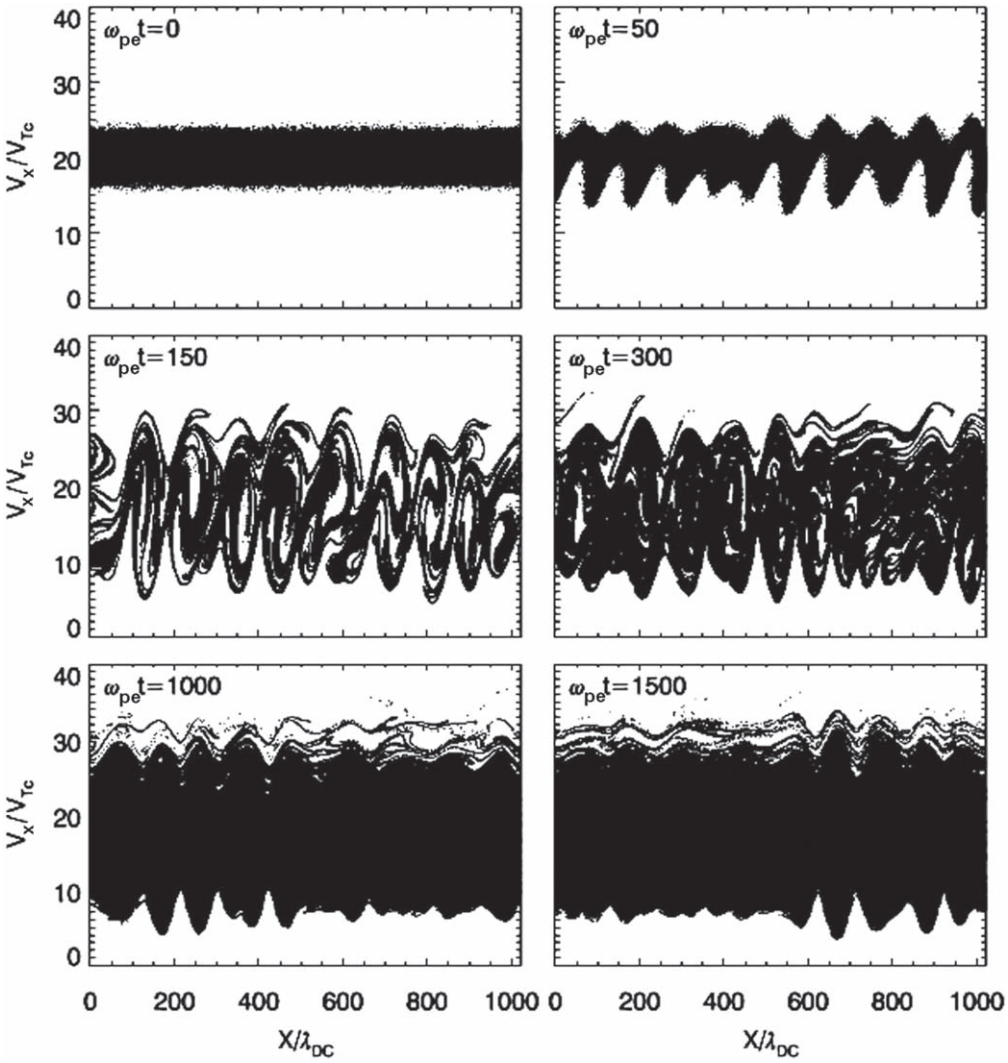

Figure 8. The phase-space (x, v_x) plots for the beam electrons at $\omega_{pe}t$ = 0, 50, 150, 300, 1 000, and 1 500 for run 3.

dispersive, where the wave modes with different wave numbers have different phase velocities. However, the trapped cold electrons and its mixing in phase space, finally, give rise to thermalization or electron heating. The heating of cold electrons is along the positive v_x direction. That may be confirmed from figure 6 by considering the time evolution plots of cold electrons in velocity space (v_x, v_y) for $\omega_{pe}t$ = 0, 150, 400, 600, 1 000, and 1 500 using the same data of run 2. It is observed that the cold electrons are only heated along the parallel component (x-axis) of the velocity during the nonlinear evolution of the wave−particle interaction.

The impact of cold electron heating on the Langmuir waves is examined in figure 7 (for run 3) with different times. It is observed that unlike figure 5, the cold electron heating does not occur. Because during this run, the EA and B waves are strongly damp, while the L waves only play their dominant role (see figure 4(b)). It is also worth mentioning that Langmuir waves are not effective for trapping and heating of cold electrons. Figure 8 illustrates the plots of phase-space (x, v_x) for beam electrons by using run 3 at different time scales $\omega_{pe}t$(=0, 100, 150, 600, 1 000, and 1 500). Initially, at $\omega_{pe}t$ = 0, the beam electrons are placed uniformly along the x-axis and do not contain any bulk velocity fluctuations. As time goes on (from $\omega_{pe}t$ = 0 to $\omega_{pe}t$ = 100), the beam electrons get somewhat trapped by the L wave. For $\omega_{pe}t$ = 150, the vortex-like structures appear with trapped beam electrons. After some time steps, the beam electrons form potential holes and later vortices, merge together and lead to the heating of the beam electrons. It is seen that Langmuir waves are more prominent mode (see figure 4(b)) and therefore more effective for trapping and heating the beam electrons. Figure 9 displays the normalized coordinates of the phase-space (x, v_x) for different normalized times $\omega_{pe}t$ (=0, 150, 400, 600, 1 000, and 1 500) using the plasma parameters of run 4. It is noticed that similar to figure 7, the cold electron trapping and heating do not occur so prominently. Because in this run, the EA waves are very weak and the B waves act as the dominant mode (see figure 4(c)). Figure 10 represents the electric field fluctuation for run 4 to give the bipolar field structures (see figure 10(a)). The solitary structures of the B wave exist at time $\omega_{pe}t$ = 1 400. The

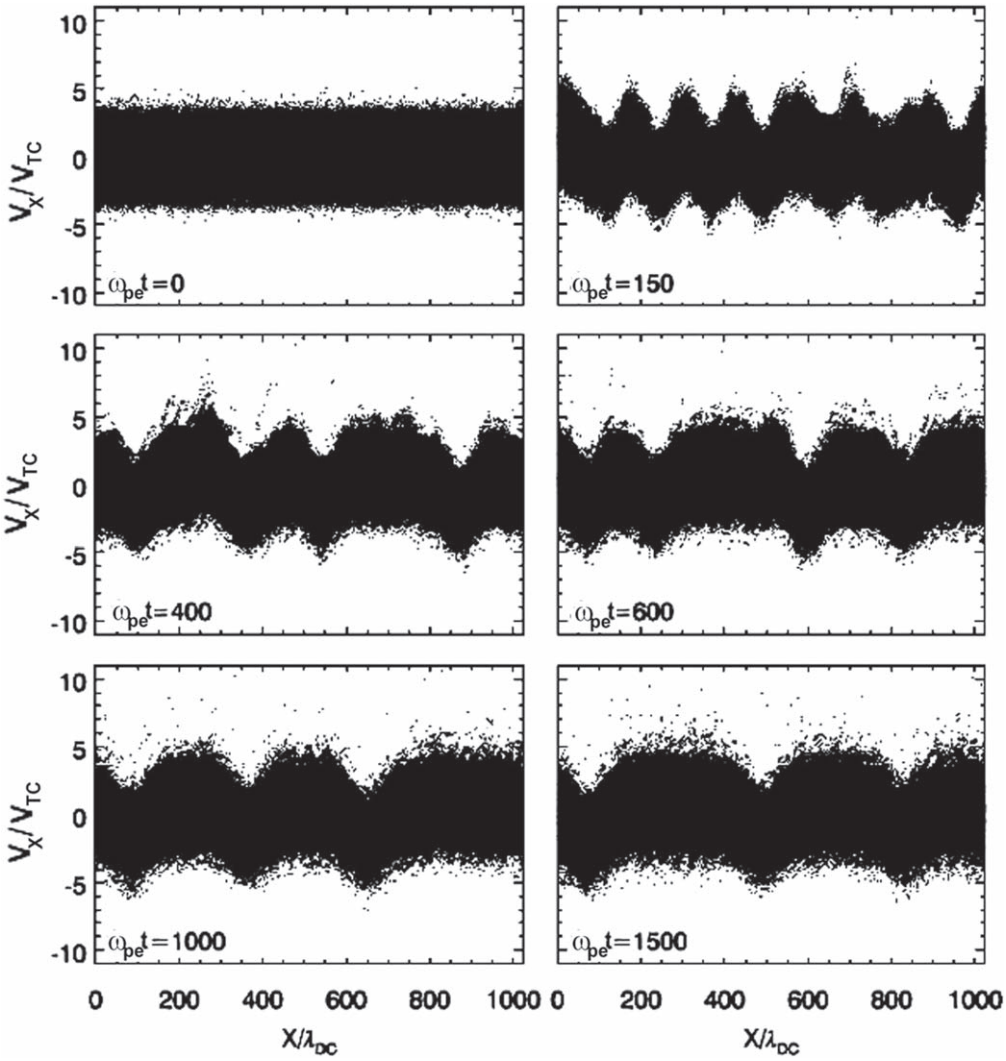

Figure 9. The phase-space (x, v_x) plots for the cold electrons at $\omega_{pe}t = 0$, 150, 400, 600, 1 000, and 1 500 for run 4.

nonlinear BGK wave mode traps the phase-space holes [38, 39]. Figure 10(b) exhibits the Fourier transformed electric field E_k versus the wavenumber k for run 4. In this figure, the values $\omega_{pe}t = 45$ and $\omega_{pe}t = 1500$ relate to the linear growth and nonlinear stages, respectively. Note that the peak of the electric field shifts toward the origin at $\omega_{pe}t = 1500$, which exactly agrees with the nonlinear behavior of waves.

4. Summary

We have employed an electrostatic 1D PIC simulation model to examine the nonlinear effects of electron-acoustic waves in a multispecies plasma, whose components are hot electrons, cold electrons, and beam electrons with immobile neutralized positive ions. For finite times, the wave–particle interaction leads to nonlinear structures in the form of vortices. When the waves saturate, as a consequence, the maximum plasma particles become trapped in the wave and trapping vortices appear more prominent. It is noted that when the electron-acoustic wave acts a dominant mode having sufficiently large amplitude, then it tends to trap cold electrons more effectively. Because the electron-acoustic waves have dispersive properties and different wavenumbers they have different phase velocities. However, the trapped cold electrons and their mixing in phase space, finally, give rise to thermalization or electron heating. It is found that (i) the electron-acoustic waves trap and heat the cold electrons more effectively, (ii) the Langmuir waves trap and heat the beam electrons more effectively but the cold electron heating does not occur, and (iii) the heating and trapping of cold electrons by beam driven waves are also not very prominent like the electron-acoustic waves.

In addition, solitary structures are formed for a large value of electron beam density. The characteristics of these solitary waves exactly coincide with the work of Omura *et al* [40, 41]. Quite recently, solitary waves with finite amplitude have been confirmed in the observations of FAST and POLAR satellites [42, 43], and these have also revealed that

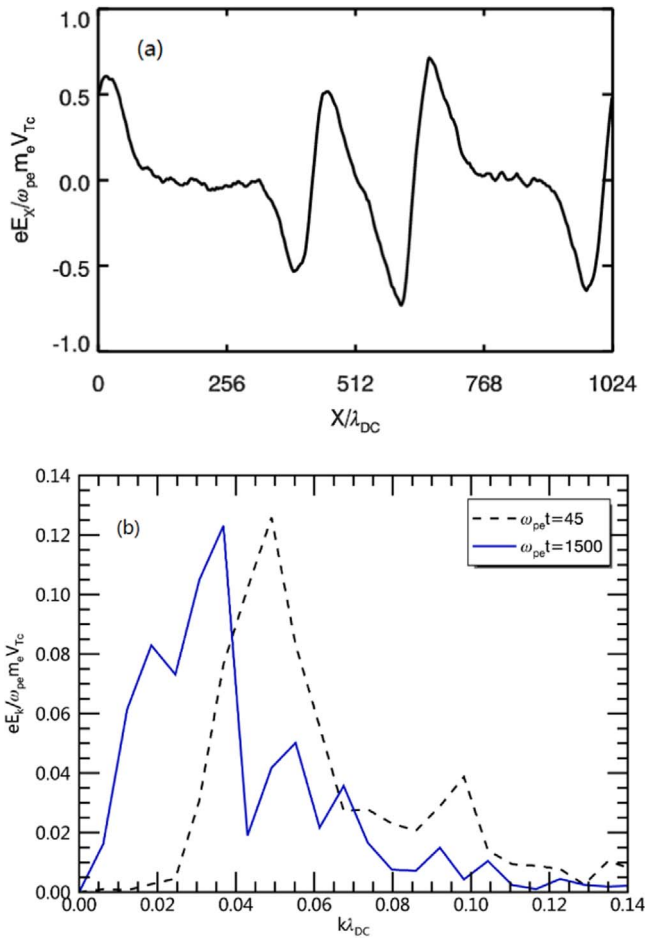

Figure 10. (a) Normalized electric field E_x versus x at $\omega_{pe}t = 1\,400.0$, (b) normalized electric field E_k versus k at $\omega_{pe}t = 45$ and 1500 for run 4.

electrostatic waves can be excited by using the beam plasma model to produce waves of broad frequencies, which may justify the BEN spectrum in the auroral region.

Acknowledgments

A A Abid acknowledges the support from Chinese Academy of Science (CAS) and TWAS for his Ph.D studies at the University of Science and Technology of China in the category of a 2016 CAS-TWAS President's Fellowship Awardee (Series No. 2016-172). This work was also partially supported by National Natural Science Foundation of China (Nos. 41331067, 41774169, and 41527804), and the Key Research Program of Frontier Sciences, CAS (QYZDJ-SSW-DQC010).

References

[1] Mace R L and Hellberg M A 1990 *J. Plasma Phys.* **43** 239
[2] Valentini F, O'Neil T M and Dubin D H E 2006 *AIP Conf. Proc.* **862** 3
[3] Rehman A *et al* 2016 *Phys. Plasmas* **23** 082122
[4] Mamun A A, Shukla P K and Stenflo L 2002 *Phys. Plasmas* **9** 1474
[5] Roth I and Hudson M K 1986 *J. Geophys. Res.* **91** 8001
[6] Thomsen M F *et al* 1983 *J. Geophys. Res.* **88** 3035
[7] Mace R L and Hellberg M A 1993 *J. Geophys. Res.* **98** 5881
[8] Ergun R E *et al* 2001 *Phys. Rev. Lett.* **87** 045003
[9] Fried D B and Gould R W 1961 *Phys. Fluids* **4** 139
[10] Watanabe K and Taniuti T 1977 *J. Phys. Soc. Jpn.* **43** 1819
[11] Landau L D 1946 *J. Phys. (Moscow)* **10** 25
[12] Summers D and Thorne R M 1991 *Phys. Fluids* B **3** 1835
[13] Rehman A and Lee J K 2018 *Phys. Plasmas* **25** 022107
[14] Gary S P and Tokar R L 1985 *Phys. Fluids* **28** 2439
[15] Tokar R L and Gary S P 1984 *Geophys. Res. Lett.* **11** 1180
[16] Yu B *et al* 2018 *Chin. J. Geophys.* **61** 3536 (in Chinese)
[17] Ergun R E *et al* 1998 *Geophys. Res. Lett.* **25** 2041
[18] Cattell C A *et al* 1999 *Geophys. Res. Lett.* **26** 425
[19] Dubouloz N *et al* 1991 *Geophys. Res. Lett.* **18** 155
[20] Singh S V, Reddy R V and Lakhina G S 2009 *Adv. Space Phys.* **43** 1940
[21] El-Taibany W F and Moslem W M 2005 *Phys. Plasmas* **12** 032307
[22] Matsukiyo S, Treumann R A and Scholer M 2004 *J. Geophys. Res.* **109** A06212
[23] Berthomier M *et al* 2000 *Phys. Plasmas* **7** 2987
[24] Lu Q M, Wang S and Dou X K 2005 *Phys. Plasmas* **12** 072903
[25] Landau L D and Lifshitz E M 1959 *Fluid Mechanics* (New York: Pergamon)
[26] Sagdeev R Z 1966 *Rev. Plasma Phys.* **4** 23
[27] Montgomery D 1967 *Phys. Rev. Lett.* **19** 1465
[28] Heinrich J, Kim S H and Merlino R L 2009 *Phys. Rev. Lett.* **103** 115002
[29] Schamel H 2000 *Phys. Plasmas* **7** 4831
[30] Abdelwahed H G and El-Shewy E K 2016 *Phys. Plasmas* **23** 082118
[31] Abdelwahed H G, El-Shewy E K and Mahmoud A A 2016 *Chin. Phys. Lett.* **33** 115201
[32] El-Hanbaly A M *et al* 2015 *Commun. Theor. Phys.* **64** 529
[33] Hafez M G *et al* 2016 *Phys. Plasmas* **23** 082904
[34] Chen F F 1974 *Introduction to Plasma Physics* (New York: Plenum Press)
[35] Schriver D 2000 *J. Geophys. Res.* **105** 12919
[36] Treumann R A and Baumjohann W 1997 *Advanced Space Plasma Physics* (London: Imperial College Press)
[37] Lu Q M and Cai D S 2001 *Comput. Phys. Commun.* **135** 93
[38] Goldman M V, Oppenheim M M and Newman D L 1999 *Geophys. Res. Lett.* **26** 1821
[39] Oppenheim M, Newman D L and Goldman M V 1999 *Phys. Rev. Lett.* **83** 2344
[40] Omura Y, Kojima H and Matsumoto H 1994 *Geophys. Res. Lett.* **21** 2923
[41] Omura Y *et al* 1996 *J. Geophys. Res.* **101** 2685
[42] Franz J R, Kintner P W and Pickett J S 1998 *Geophys. Res. Lett.* **25** 1277
[43] Tsurutani B T *et al* 1998 *Geophys. Res. Lett.* **25** 4117